THE JOURNAL OF BIOLOGICAL CHEMISTRY VOL. 288, NO. 4, pp. 2271–2280, January 25, 2013
Published in the U.S.A.

Identification of a Novel Site in the Tail of Dynein Heavy Chain Important for Dynein Function *in Vivo*[*][S]

Received for publication, August 22, 2012, and in revised form, November 28, 2012 Published, JBC Papers in Press, December 3, 2012, DOI 10.1074/jbc.M112.412403

Rongde Qiu, Jun Zhang, and Xin Xiang[1]

From the Department of Biochemistry and Molecular Biology, the Uniformed Services University of the Health Sciences, Bethesda, Maryland 20814

Background: The dynein heavy chain tail is required for subunit interactions but not for *in vitro* motility.
Results: A dynein tail mutation affects dynein function *in vivo* without affecting subunit interactions.
Conclusion: A site upstream of the subunit interaction sites of the dynein tail is important *in vivo*.
Significance: This study discovers a novel site of the dynein tail critical for motor function *in vivo*.

The minus end-directed microtubule motor cytoplasmic dynein is responsible for the intracellular movements of many organelles, including nuclei and endosomes. The dynein heavy chain contains a C-terminal motor domain and an N-terminal tail domain. The tail binds other dynein subunits and the cargo-interacting dynactin complex but is dispensable for movement of single dynein molecules *in vitro*. Here, we identified a mutation in the *Aspergillus nidulans* heavy chain tail domain, *nudA*^{F208V}, which causes obvious defects in dynein-mediated nuclear positioning and early endosome movement. Astonishingly, the *nudA*^{F208I} mutation in the same position does not cause the same defects, suggesting that a subtle difference in the size of the amino acid side chain at this position has a significant consequence. Importantly, our biochemical analyses indicate that the *nudA*^{F208V} mutation does not affect dynein subunit interactions and the mutant dynein is also able to bind dynactin and another dynein regulator, NUDF/LIS1. The mutant dynein is able to physically interact with the early endosome cargo, but dynein-mediated early endosome movement away from the hyphal tip occurs at a significantly reduced frequency. Within the small group of early endosomes that move away from the hyphal tip in the mutant, the average speed of movement is lower than that in the wild type. Given the dispensability of the dynein tail in dynein motility *in vitro*, our results support the notion that the structural integrity of the dynein tail is critical *in vivo* for the coordination of dynein force production and movement when the motor is heavily loaded.

Cytoplasmic dynein, a minus end-directed microtubule motor, is important for a variety of cellular functions, including organelle positioning and the intracellular transport of vesicles, proteins, and viruses (1–6). Defects in cytoplasmic dynein and its regulatory proteins such as dynactin (7) or LIS1 (8) cause neurodegenerative and neurodevelopmental disorders (8, 9). The dynein heavy chains (HCs)[2] within the dynein complex form a dimer that contains motor activity responsible for ATP-dependent movement of dynein along microtubules. Each HC contains a C-terminal motor domain that forms a ring containing six AAA (ATPase of various cellular activities) domains and a microtubule-binding stalk located in between AAA4 and AAA5 (10–13). The N terminus of the HC is called the "tail" (or the "stem"), which is implicated in dynein HC dimerization and binding to other subunits, including intermediate chains (ICs), light intermediate chains (LICs), and light chains (14). The dynein IC contains binding sites for the light chains, dynactin, and another dynein regulator NudE that recruits LIS1 (14–26). Although the linker region immediately before the AAA1 domain is involved in power stroke, the HC tail N-terminal to the subunit-interaction site is not important for movements of single dynein molecules *in vitro* (27–31). It has been proposed, however, that the tail plays a role in regulating dynein motor function (32). This hypothesis is supported by the results that the neurodegenerative mutation *Loa* (legs at odd angles, F580Y in mouse HC) in the HC tail affects dynein motor processivity (32) or velocity (33). However, because defects in dynein subunit interactions and/or interaction with dynactin have been detected in the *Loa* mutant (32, 34), the contribution of other factors to the *Loa* phenotype is hard to be completely excluded.

The filamentous fungus *Aspergillus nidulans* is an excellent genetic system for studying intracellular trafficking and the regulation of cytoplasmic dynein (35–38). In *A. nidulans*, components of the dynein-dynactin complexes and other regulators, including LIS1 and NudE/Nudel, are required for *nud* (nuclear distribution), and loss of function of these proteins produces a *nud* phenotype (19, 36, 39). In addition to its function in nuclear distribution, dynein in filamentous fungi is also critical for the retrograde movement of early endosomes in hyphae as first discovered in *Ustilago maydis* (35–38, 40). In *A. nidulans*, as well as in *Saccharomyces cerevisiae*, *U. maydis*, and mammalian cells, dynein forms comet-like structures, representing their accumulation at the microtubule plus ends (40–44). In *A. nidulans* and *U. maydis*, this accumulation at the microtu-

* This work was supported by the National Institutes of Health (1RO1GM097580-01), the Center for Neuroscience and Regenerative Medicine, Department of Defense, and a Uniformed Services University of the Health Sciences intramural grant.

[S] This article contains supplemental Movies 1–8.

[1] To whom correspondence should be addressed: Dept. of Biochemistry and Molecular Biology, the Uniformed Services University of the Health Sciences, Bethesda, MD. Tel.: 301-295-0000; Fax: 301-295-3512; E-mail: xin.xiang@usuhs.edu.

[2] The abbreviations used are: HC, heavy chain; IC, intermediate chain; LIC, light intermediate chain.

This is an Open Access article under the CC BY license.

TABLE 1
***A. nidulans* strains used in this study**

Strain name	Genotype	Source
GR5	*pyrG*89; *pyroA*4; *wA*3	G. S. May
TNO2A3	Δ*nkuA*::*argB*; *pyrG*89; *pyroA*4	Ref. 80
JZ11 or S-IC	S-tagged-*nudI*; *pyrG*89; *pabaA*1, *yA*1	Ref. 57
LZ12	GFP-*nudA*; *nkuA*::*argB*; *pyroA*4; *pyrG*89	Ref. 57
LZ26	GFP-*nudA*; S-tagged-*nudI* (or S-IC); *nkuA*::*argB*; *pyroA*4; *pyrG*89, *yA*1	Ref. 57
XX222	GFP-*nudA*; *argB*2::[*argB**-*alcAp*::mCherry-*RabA*]; *pantoB*100	Ref. 47
JZ476	GFP-*nudA*^{F208V}; S-IC; *wA*2; possibly *pyroA*4; possibly *pabaA*1; possibly *yA*1	This work
RQ2	GFP-*nudA*; *argB*2::[*argB**-*alcAp*::mCherry-*RabA*]; *nkuA*::*argB*; *pyrG*89; *pyroA*4; *yA*1	This work
RQ5	GFP-*nudA*^{F208V}; *argB*2::[*argB**-*alcAp*::mCherry-*RabA*]; pyrG89; *pyroA*4; *wA*2	This work
RQ8	GFP-*nudA*^{F208V}; *argB*2::[*argB**-*alcAp*::mCherry-*RabA*]; pyrG89; *wA*2	This work
RQ16	GFP-*nudA*; *argB*2::[*argB**-*alcAp*::mCherry-*RabA*]; *nkuA*::*argB*; *pyrG*89; *wA*2 (with pAid)	This work
RQ39	GFP-*nudA*^{F208I}; *argB*2::[*argB**-*alcAp*::mCherry-*RabA*]; pyrG89; *wA*2 (with pAid)	This work
RQ47	GFP-*nudA*$^{F208V, T1133S}$; *argB*2::[*argB**-*alcAp*::mCherry-*RabA*]; pyrG89; *wA*2	This work
RQ49	GFP-*nudA*$^{F208V, N356K}$; *argB*2::[*argB**-*alcAp*::mCherry-*RabA*]; pyrG89; *wA*2	This work
RQ54	*argB*2::[*argB**-*alcAp*::mCherry-*RabA*]; *nkuA*::*argB*; *pyrG*89; *pyroA*4; *wA*2	This work

bule plus ends near the hyphal tip facilitates dynein-early endosome interaction, and thus is important for dynein-driven transport of early endosomes from the hyphal tip (37, 40, 45–47). The plus-end accumulation of dynein depends on the integrity of the dynein-dynactin complexes and kinesin-1 (40, 48–53). Loss of IC abolishes plus-end comet formation (48), presumably because dynein could no longer bind to p150 dynactin (15–17), a key factor in the plus-end localization of *A. nidulans* dynein (52, 53). Loss of LIC also abolishes plus-end comet formation because HC-IC interaction is significantly weakened in the absence of LIC (50).

In this current study, we have identified a HC tail mutation that does not affect the accumulation of dynein at the microtubule plus ends but causes obvious defects in dynein-mediated early endosome transport and nuclear migration. This mutation, *nudA*^{F208V}, is far upstream from the previously mapped IC- and LIC-binding site, and our experimental data demonstrate that it does not affect dynein complex formation or dynein-early endosome interaction. Interestingly, changing the valine residue to isoleucine completely rescues the mutant phenotype, suggesting that a subtle change in the size of the side chain of this residue is sufficient for causing a significant effect on HC function *in vivo*. Thus, beyond the known role of the HC tail in interacting with other dynein subunits implicated in cargo binding, a novel site upstream of the subunit interaction site plays a significant role in dynein motor function *in vivo*.

EXPERIMENTAL PROCEDURES

A. nidulans Strains, Media, and Mutagenesis—*A. nidulans* strains used in this study are listed in Table 1. For biochemical experiments, YG (yeast extract plus glucose) + uridine + uracil (or YUU) liquid medium was used. UV mutagenesis on spores of *A. nidulans* strains was done as described previously (54, 55). For DAPI staining of nuclei, cells were incubated in YUU medium for 8 h at 37 °C. For live cells imaging experiments, liquid minimal medium plus supplements was used, and cells were cultured at 32 °C for overnight and observed at room temperature.

For observing early endosome movement *in vivo*, we used a minimal medium containing either 1% glycerol (v/v) or 0.9% (w/v) fructose and 6.25 mM threonine (56). For observing GFP-HC, we also used these two types of minimal media, and in addition, we used a minimal medium containing either 0.1% (w/v) glucose or 1% glucose.

Identification of the nudA^{F208V} *Mutation and Creation of the nudA*^{F208I} *Mutation*—The *nudA* sequence of the 4-63 mutant corresponding to the wild type *nudA* fragment that complemented the 4-63 mutant was sequenced using primers as described previously (57), which led to the identification of the *nudA*^{F208V} mutation. To construct the mutant strain carrying the *nudA*^{F208I} mutation, we first made the DNA fragment containing this mutation using fusion PCR. Specifically, two fragments were made using the primer pairs of NudA51 (AAAACTCTATCTGCCCGCGAA) and FIR (GAGTTCCAGCTCCGCGATTTTCTTCTTAGTGCC), and of NudA33 (CAATGGAAATCTGATAACGCG) and FIF (GGCACTAAGAAGAAAATCGCGGAGCTGGAACTC) respectively, followed by a fusion PCR using the primer pair of NudA51 and NudA33. This fragment was transformed into the RQ8 strain containing the *nudA*^{F208V} mutation, and wild type-looking transformants were subjected to sequencing analysis.

Identification of Suppressors of the nudA^{F208V} *Mutation*—We performed a UV mutagenesis on the RQ8 strain containing the *nudA*^{F208V} mutation. UV mutagenesis on spores of the RQ8 strain was done as described previously (54, 55). Colonies that looked healthier than that of the *nudA*^{F208V} mutant were judged to be suppressors and selected from the plates. Two suppressors were selected and crossed with a wild type strain. We did not see any *nudA*^{F208V}-like colonies among the progeny, suggesting that the suppressor mutations are linked to the original *nudA*^{F208V} mutation. These suppressors were further analyzed by sequencing of the *nudA* gene. Primers for sequencing were as described previously (57).

Live Cell Image Analyses—Fluorescence microscopy of live *A. nidulans* cells was as described (47, 52). Cells were grown at 32 °C overnight using the Lab-Tek chambered cover-glass system. Images were captured at room temperature using an Olympus IX70 inverted fluorescence microscope (with a 100× objective) linked to a PCO/Cooke Corp. Sensicam QE cooled CCD camera. A filter wheel system with GFP/mCherry-ET Sputtered series with high transmission (BioVision Technologies) was used. The IPLab software was used for image acquisition and analysis.

Analyses of Protein-protein Interactions, Sucrose Gradient Centrifugation, and Western Blotting—Dynein HC-IC interactions were examined using strains containing a functional S-tagged dynein IC as done previously (57). Alternatively, the

μMACS GFP isolation kit (Miltenyi Biotec) was used to determine whether GFP-tagged dynein HC pulls down IC. About 0.7 g of hyphal mass was harvested from overnight culture for each sample, and cell extract was prepared using a lysis buffer containing 25 mM Tris-HCl, pH 8.0, 0.4% Triton X-100, 0.3% (v/v) of a protease inhibitor mixture (Sigma-Aldrich), and 0.1% (v/v) of a phosphatase inhibitor mixture (Sigma-Aldrich). Cell extract was centrifuged at 16,000 × *g* for 30 min at 4 °C, and supernatant was used for the pulldown experiment. To pull down GFP-tagged protein, 50 μl of anti-GFP MicroBeads were added into the cell extract and incubated on ice for 30 min. The MicroBeads/cell extract mixture was then applied to the column provided with the GFP isolation kit, followed by gentle wash with the lysis buffer. After washing four times with the lysis buffer, the column was finally washed one more time with the lysis buffer without any detergent. The preheated (95 °C) SDS-PAGE sample buffer was used as an elution buffer. For analyzing dynein complex sedimentation using sucrose gradient centrifugation, the cell extract was centrifuged at 100,000 × *g*, and the supernatant was loaded on the top of a 5–25% sucrose step gradient and centrifuged at 4 °C overnight at 100,000 × *g* using the SW41 rotor. Fractions were collected from the top and analyzed on protein gels. Thymoglobulin (Sigma-Aldrich) was used as a 19 S marker. Antibodies against dynein HC, dynein IC, p150 dynactin, and NUDF/LIS1 were described previously (39, 51, 58). Anti-GFP antibodies from Covance (monoclonal) and Clontech (polyclonal) were also used for Western analyses. Western analyses were performed using the alkaline phosphatase system, and blots were developed using the AP color development reagents from Bio-Rad.

Analyses of Dynein-early Endosome Interaction—For the biochemical analyses of dynein-early-endosome interaction, we used the strains containing GFP-labeled dynein HCs and mCherry-RabA-labeled early endosomes. The strains were grown overnight in the liquid minimal medium containing 0.9% (w/v) fructose and 50 mM threonine, which induces the expression of the mCherry-RabA fusion under the control of the *alcA* promoter. About 0.7 g of hyphal mass was harvested from overnight culture for each sample, and cell extract was prepared using a lysis buffer containing 25 mM Tris-HCl, pH 8.0, 0.01% Triton X-100, 0.3% (v/v) of a protease inhibitor mixture (Sigma-Aldrich), and 0.1% (v/v) of a phosphatase inhibitor mixture (Sigma-Aldrich). Cell extract was centrifuged at 4,000 × *g* for 30 min at 4 °C, and supernatant was used for the pulldown assay using the μMACS GFP isolation kit (Miltenyi Biotec). As described earlier, 50 μl of anti-GFP MicroBeads were added into the cell extract and incubated on ice for 30 min. The MicroBeads/cell extract mixture was then applied to the column provided with the GFP isolation kit, followed by gentle wash with the lysis buffer five times. Preheated (95 °C) SDS-PAGE sample buffer was used as an elution buffer. The anti-mCherry antibody used on the Western blots to detect mCherry-RabA was purchased from BioVision Research Products. Western analyses were performed using the alkaline phosphatase system, and blots were developed using the AP color development reagents from Bio-Rad. Quantification of the protein band intensity was done using the IPLab software as described previously (52), with a minor modification. Specifically, an area containing the whole band was selected as a region of interest, and the intensity sum within the region of interest was measured. Then, the region of interest box was dragged to the equivalent region of the negative control lane to take the background value, which was then subtracted from the intensity sum. The intensity ratio of the pulled down mCherry-RabA to GFP-HC was calculated. The ratios calculated from the wild type samples were set as 1, and the relative ratios of the mutant were calculated and presented.

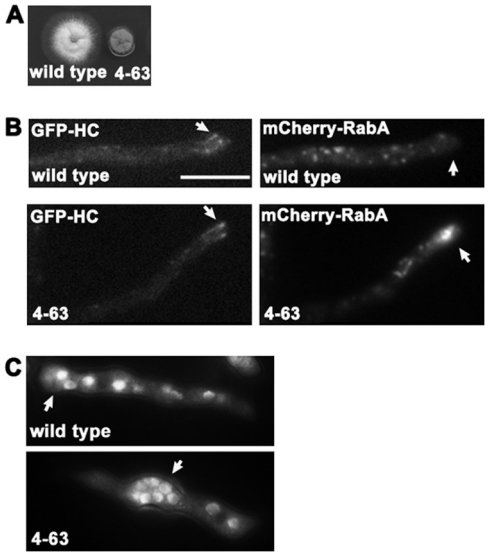

FIGURE 1. **Phenotypes of the 4-63 (later identified as *nudA*^{F208V}) mutant.** *A*, the mutant forms a colony that is smaller than wild type. *B*, the mutant exhibits normal dynein localization to microtubule plus ends as evidenced by the presence of comet-like structures near the hyphal tip (indicated by *arrows*), but it shows a severe defect in the retrograde movement of early endosomes as evidenced by an abnormal accumulation of the mCherry-RabA signals at the hyphal tip. (The hyphal tips in the wild type and the mutant are indicated by *arrows*.) *C*, the mutant exhibits an obvious defect in nuclear distribution as evidenced by DAPI staining showing a cluster of multiple nuclei in the spore head (the spore heads in the wild type and the mutant are indicated by *arrows*). *Bar*, 5 μm.

RESULTS

The nudA^{F208V} *but Not nudA*^{F208I} *Mutation Causes a Defect in Dynein Function*—To study the regulation of dynein-mediated retrograde transport of early endosomes, we used UV mutagenesis to obtain mutants that are defective in early endosome transport. The strain we used for mutagenesis contains the GFP-*nudA* allele that replaces the endogenous *nudA* and reports HC localization (57) and the mCherry-RabA allele that reports the distribution of early endosomes (45, 47). One mutant we selected was called 4-63, which formed a colony smaller than the wild type (Fig. 1*A*). In this mutant, GFP-HC formed normal comet-like structures near the hyphal tip (Fig. 1*B*, *arrows*), which represent dynein accumulation at the microtubule plus ends (41). However, a prominent buildup of mCherry-RabA-labeled early endosomes was observed in almost every hyphal tip, indicating a defect in dynein-mediated retrograde transport of early endosomes (Fig. 1*B*, *arrows*). The mutant also exhibited an obvious defect in nuclear distribution (Fig. 1*C*). Specifically, a cluster of multiple nuclei in the spore head was often observed (Fig. 1*C*, *arrows*). This phenotype differs from that of the null mutant of p25, a dynactin subunit

required for dynein-early endosome interactions but not for nuclear positioning (59). Based on this phenotype, we concluded that the corresponding protein, unlike p25, is likely to be required for dynein activity rather than being specifically required for the physical interaction of dynein with early endosomes.

During an analysis of more than 50 progenies from a cross between the GFP-HC-containing mutant and a wild type strain without GFP-HC, we noticed that the mutant phenotypes of colony growth and early endosome accumulation were always linked with each other and also with the presence of plus-end comet signals formed by GFP-HC. This suggests that the colony phenotype and the defect in early endosome transport are caused by the same mutation located within or very close to the *nudA* gene encoding dynein HC.

To identify the mutation, we first prepared five different wild type genomic DNA fragments covering the entire 14-kb *nudA* gene by using high-fidelity PCR. Each *nudA* fragment was then co-transformed into the mutant with the auto-replicating pAid plasmid containing the selective marker gene *pyrG* (55). The 3-kb fragment containing sequences encoding the N-terminal part of HC was able to rescue the mutant phenotype via homologously replacing the equivalent sequence in the mutant genome. The corresponding region of the mutant was fully sequenced, and one single mutation, T622G (in the coding sequence), was found when compared with the wild type *nudA* sequence (Fig. 2*A*). Sequencing of five more individual mutant progenies from a cross further confirmed the identity of this mutation. This mutation results in a change in the amino acid residue 208 from phenylalanine (Phe) to valine (Val).

The *nudA*^{F208V} mutation is located in the tail of the dynein HC (Fig. 2*B*). An alignment of dynein HC sequences from various organisms showed that although this region is conserved to certain extent, this phenylalanine residue is changed to leucine (Leu) or isoleucine (Ile) in some species (Fig. 2*C*). Because the side chains of these amino acids are longer than that of valine, we hypothesized that a subtle difference in the size or hydrophobicity of the side chain may be responsible for the observed phenotype produced by the *nudA*^{F208V} mutation. To test this, we mutated the F208 residue to isoleucine that also contains a branched side chain like valine but contains one extra $-CH_3$ group. We made a DNA fragment containing the codon change of *nudA*^{F208I} and introduced it to the *nudA*^{F208V} mutant. This fragment was able to rescue the mutant via homologous recombination and produce a colony essentially identical to wild type (Fig. 2*D*). The *nudA*^{F208I} mutant also exhibited normal nuclear distribution and early endosome distribution (Fig. 2, *E* and *F*). The striking phenotypic difference between the *nudA*^{F208V} mutant and the *nudA*^{F208I} mutant indicates that a subtle change in the side chain of Phe-208 makes a significant difference in the function of dynein HC.

The nudA^{F208V} *Mutation in the Dynein Tail Does Not Affect Dynein Complex Assembly, but Affects the Cargo-transporting Capacity of Dynein*—The *nudA*^{F208V} mutation locates at a site far upstream of the linker region before AAA1 implicated in motor activity, and it is also more upstream of the subunit interaction sites within the HC tail. Previous *in vitro* studies mapped the sites of HC dimerization, HC-IC interaction, and HC-LIC interaction to the tail region of the HC. These studies were done using *in vitro*-expressed HC fragments of cytoplasmic dynein HCs from rat and *Dictyostelium discoideum* (60, 61). The HC dimerization site on the rat HC was mapped to a big region containing amino acids 300–1140 (60), which corresponds to a region containing amino acids 325–1180 of *A. nidulans* HC. However, the study using *Dictyostelium* HC fragments mapped the dimerization site to a region containing amino acids 627–780 (61), corresponding to amino acids 603–759 of *A. nidulans* HC. The IC binding site within the *D. discoideum* HC is in a region containing amino acids 629–730 (61), corresponding to amino acids 605–690 of the *A. nidulans* HC. However, the IC binding site of the rat HC contains amino acids 446–701 (60), corresponding to amino acids 470–720 of *A. nidulans* HC. Within the rat HC, the LIC binding site contains amino acids 649–800 (60), which correspond to amino acids 668–816 of *A. nidulans* HC. All of these sites are downstream of the *nudA*^{F208V} mutation that we identified.

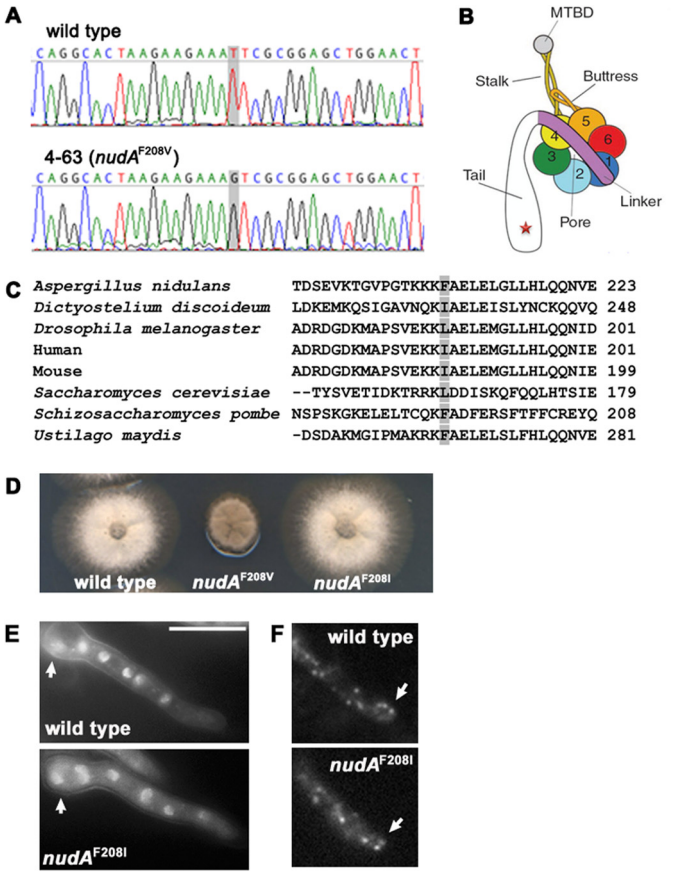

FIGURE 2. **Identification of the *nudA*^{F208V} mutation as the 4-63 mutation in dynein HC.** *A*, sequence of the mutant genomic DNA showing the T622G mutation in the coding region of *nudA*. This change is predicted to cause the *nudA*^{F208V} mutation in the HC tail. *B*, a diagram showing the position of the mutation in the HC tail (*red star*). The original diagram was published in Schmidt *et al.* (74). *C*, a sequence alignment showing that the Phe-208 residue is conserved in some species but changed to other amino acids such as isoleucine and leucine in the dynein HCs of other organisms. *D*, the *nudA*^{F208I} mutant forms a wild type colony. *E*, the *nudA*^{F208I} mutant exhibits normal nuclear distribution with no cluster of multiple nuclei in the spore head. The spore heads are indicated by *arrows*. *F*, the *nudA*^{F208I} mutant exhibits normal early endosome distribution with no buildup of early endosomes at the hyphal tip. The hyphal tips are indicated by *arrows*. *Bar*, 5 μm.

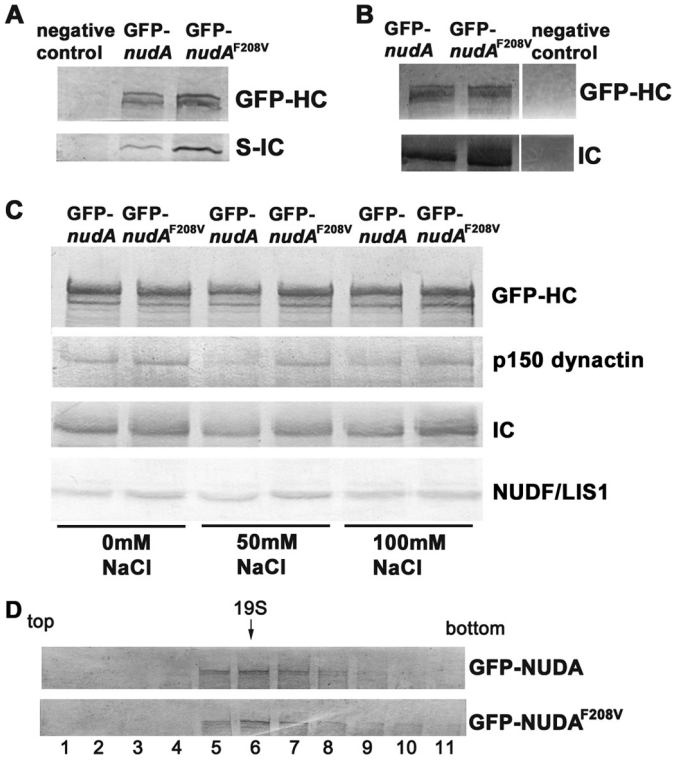

FIGURE 3. **The *nudA*^{F208V} mutation does not weaken the HC-IC, dynein-dynactin, or dynein-NUDF/LIS1 interaction.** *A*, the amount of the *nudA*^{F208V} mutant HC pulled down with the S-tagged IC (*S-IC*) is normal compared with that of the wild type HC. The lane labeled as "negative control" contains the sample from a wild type strain whose IC is not tagged with the S-tag. *B*, the amount of IC pulled down by the GFP-antibody from the extract containing GFP-*nudA*^{F208V} is normal compared with that from the extract containing GFP-*nudA*. The lane labeled as negative control contains the sample from a wild type strain whose HC is not tagged with GFP. The experiment was done using a protein extraction buffer containing detergent but no NaCl. *C*, the amount of dynein IC, p150 of dynactin or NUDF/LIS1 pulled down by the GFP-antibody from the extract containing GFP-*nudA*^{F208V} is similar to that from the extract containing GFP-*nudA*. The experiment was done using a protein extraction buffer containing 0 mM, 50 mM, or 100 mM NaCl. *D*, the mutant HC is incorporated into the dynein complex as indicated by its normal sedimentation at ~19 S in a 5–25% sucrose gradient. The experiment was done using a protein extraction buffer containing 50 mM NaCl.

In addition to the positions of the deduced subunit binding sites in *A. nidulans* HC, several lines of experimental evidence also helped us to exclude the possibility that the *nudA*^{F208V} mutation affects the HC-IC and/or HC-LIC interactions. First, although loss of IC or LIC in *A. nidulans* abolishes microtubule plus-end comets formed by the dynein HC (48, 50), GFP-NUDA^{F208V} formed comet-like structures just like wild type HCs (Fig. 1*B*). Second, HC was pulled down with S-tagged IC from extract isolated from the *nudA*^{F208V} mutant (Fig. 3*A*). Similarly, the amount of IC associated with GFP-NUDA^{F208V} was normal as judged by pulldown experiments using a GFP-antibody coupled to magnetic beads (Fig. 3*B*), and the same conclusion was obtained even when the pulldown experiments were performed using high-salt buffers (Fig. 3*C*). Because loss of dynein LIC is known to abolish HC-IC interaction (50), we concluded that neither HC-IC nor HC-LIC interaction is weakened by the *nudA*^{F208V} mutation. This conclusion was further confirmed by a sucrose gradient sedimentation experiment showing normal sedimentation of the mutant dynein complex (Fig. 3*D*). Thus, we have identified a novel mutation in the dynein tail that clearly affects dynein function but not dynein complex assembly. In addition, our biochemical data also indicate that the *nudA*^{F208V} mutation does not weaken the dynein-dynactin interaction (Fig. 3*C*), which is expected because IC is the subunit that binds to dynactin (15–17) and because dynein forms normal plus-end comets (Fig. 1*B*), which is dynactin-dependent (49, 51–53). Moreover, the *nudA*^{F208V} mutation does not affect the interaction between dynein and the LIS1 homolog NUDF (Fig. 3*C*).

To explore the mechanism of the *nudA*^{F208V} mutation, we examined dynein-mediated movements of early endosomes in more detail in both the mutant and wild type control strains. We first used a minimal growth medium containing glycerol as a carbon source, which allows the expression of the early endosome marker mCherry-RabA under the control of the *alcA* promoter. Under this condition, early endosomes were clearly blocked at the hyphal tip in the mutant as shown in Fig. 1*B*. The frequency of early endosome movement away from the hyphal tip in the mutant was about seven times lower than that in wild type. Because the number of early endosomes that move away from the hyphal tip was very low, it was not easy to do a quantitative analysis on the speed of movement in the mutant. We next used another minimal medium containing fructose and threonine, which allows a robust hyphal growth and a relatively low level of expression of the *alcA* promoter. In this medium, the signal intensity of mCherry-RabA in the wild type control was quite low compared with that in the glycerol-containing medium, most likely reflecting the relatively low expression level of the *alcA*-driven mCherry-RabA fusion protein. Under this condition, dynein-mediated movements of early endosomes were still blocked in the mutant, as evidenced by the abnormal accumulation of mCherry-RabA signals at the hyphal tip (Fig. 4*A*, supplemental Movies 1 and 2). However, more retrograde movements were observed, allowing for a quantitative analysis of the movement speed. Measurements of kymographs (Fig. 4*B*) showed that although some early endosomes in the mutant moved as quickly as those in the wild type control, the frequency of the slower early endosomes was increased. Of 53 early endosomes we measured from the mutant, nine of them (~17%) moved at a speed below 1 μm/s, which was never observed in wild type ($n = 55$) (Fig. 4*C*). Consequently, the average speed of dynein-mediated movements in the mutant was mildly reduced (Fig. 4*D*). The frequency of movements from the hyphal tip was about three times lower in the mutant than in the wild type (Fig. 4*E*). Sometimes, early endosomes in the mutant underwent short distance movements away from the tip but moved right back to the hyphal tip (supplemental Movie 3). Under these conditions, we also observed a cloud of GFP-HC signals at the hyphal tip region where early endosomes also accumulated (supplemental Movies 4–6). This cloud was also observed in the mutant grown on glucose that shuts off the expression of mCherry-RabA, but not observed in the wild type strain grown under the same conditions (supplemental Movies 7 and 8). Because early endosomes also accumulate at the hyphal tip region, this localization pattern of dynein suggests that the mutant dynein is likely to interact with early endosomes. Such an idea is consistent with the result that the mutant HC is able to bind to IC, which binds dynactin (15–17), a com-

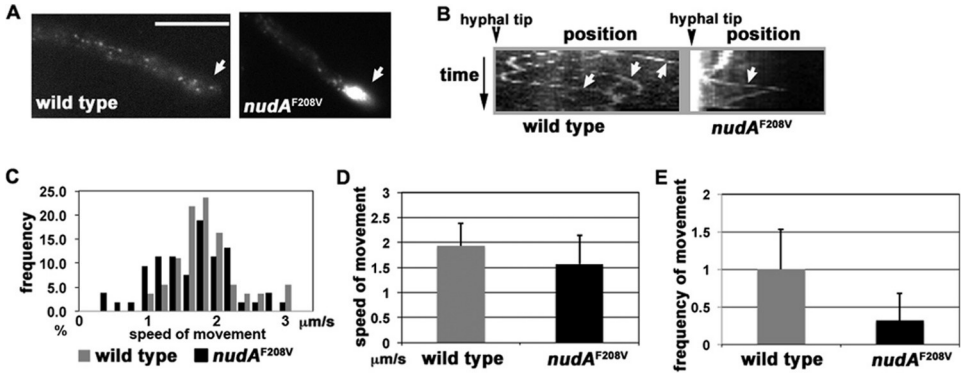

FIGURE 4. **A quantitative analysis of dynein-mediated retrograde transport of early endosomes in the *nudA*^{F208V} mutant.** *A*, images showing distribution patterns of early endosomes in the wild type and the *nudA*^{F208V} mutant strains. Positions of the hyphal tips are indicated by *arrows*. *Bar*, 5 μm. *B*, kymographs from the same time-lapse images of the wild type and mutant cells shown in *A*. *Arrows* point to the lines that represent retrograde transport from the hyphal tip. The kymograph generated from the mutant shows an early endosome that first left the hyphal tip and then came back. *C*, an analysis of the speed distribution of retrograde early endosome movement away from the hyphal tip. The percentage of early endosomes that move at various speeds is shown as the frequency value ($n = 55$ early endosomes for the wild type, and $n = 53$ for the mutant). *D*, mean and S.D. values of the speed of dynein-mediated early endosome movement away from the hyphal tip. The mean speed value of the mutant is mildly reduced ($p < 0.05$; $n = 55$ for the wild type, and $n = 53$ for the mutant). *E*, an analysis of the frequency of early endosome movements away from the hyphal tip. Mean and S.D. values are shown ($n = 68$ hyphal tips for the wild type and $n = 64$ for the mutant). The average frequency of movements in the mutant within a time period of 16 s is relative to that of the wild type, which is set as 1. The frequency is significantly lower in the mutant than in wild type ($p < 0.001$).

plex required for dynein-early endosome interaction (59, 62). To confirm this idea, we used a biochemical pulldown assay to directly examine the physical interaction between the dynein HC labeled with GFP and the early endosome cargo labeled with mCherry-RabA. The GFP antibody-conjugated magnetic beads pulled down dynein-bound early endosomes from cell extract, which were detected on Western blots probed by an anti-mCherry antibody (Fig. 5*A*). A strain containing mCherry-RabA but not GFP-HC was used as a negative control for this assay, and the amount of mCherry-RabA pulled down from the extract of this negative control strain was negligible (Fig. 5*A*). The result of this assay showed that the mutant dynein is clearly able to bind early endosomes. In fact, the amount of mCherry-RabA pulled down from the mutant extract was even higher than that from the wild type extract (Fig. 5, *A* and *B*, $p < 0.05$, $n = 3$), possibly because recycling of the mutant dynein from non-motile early endosomes is relatively inefficient. Together, our results suggest that rather than negatively affecting dynein-cargo interaction, the *nudA*^{F208V} mutation affects the ability of cargo-bound dynein in initiating or sustaining movements along microtubules *in vivo*.

Two Suppressor Mutations of the nudA^{F208V} *Mutant, nudA*^{T1133S}*, and nudA*^{N356K}*, Are also Located in the HC Tail*—To gain further insight into the structural role of the *nudA*^{F208} residue, we performed a UV mutagenesis on the *nudA*^{F208V} mutant. The spores were mutagenized as described previously and plated out on YUU plates. From ~8,000 colonies, two strains, RQ47 and RQ49, were selected. These two strains looked healthier than the original mutant on plates (Fig. 6*A*), but less healthy than the wild type, indicating only a partial recovery of dynein function. As expected, the defects in dynein-mediated early endosome transport and nuclear distribution were only partially but not fully suppressed (Fig. 6, *B*–*E*). To test whether the suppressor mutations were located in the *nudA* gene, we crossed the selected suppressor with a wild type strain. We reasoned that if the suppressor mutation is linked with *nudA*^{F208V}, none of the progeny should look like the original

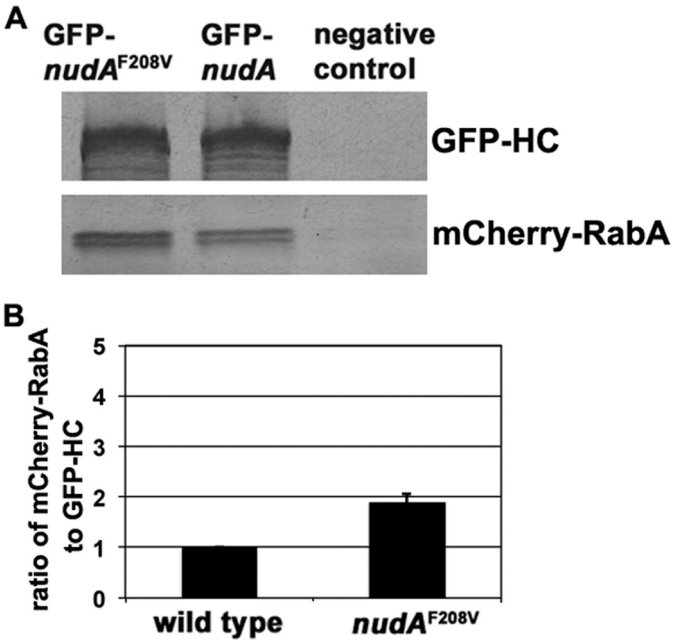

FIGURE 5. **A biochemical analysis showing that dynein in the *nudA*^{F208V} mutant is able to interact with mCherry-RabA-labeled early endosomes.** *A*, Western blots showing a result of the pulldown assay for dynein-early endosome interaction using an anti-GFP antibody conjugated to magnetic beads. The amount of mCherry-RabA pulled down with the GFP-HC from the *nudA*^{F208V} mutant extract is clearly not lower than that from the wild type extract. The lane labeled as negative control contains the pulldown sample from a strain containing mCherry-RabA but not GFP-HC. *B*, a quantitative analysis of the results of the pull-down assays for dynein-early endosome interaction. The intensity ratio of the mCherry-RabA band to that of the GFP-HC band is shown. The value of the mutant is relative to the wild type values, which is set at 1. Mean and S.D. values were calculated from three independent pulldown experiments.

mutant. This turned out to be the case for both suppressors. To identify the suppressor mutation in RQ47, we sequenced the entire *nudA* gene from the selected suppressor mutant. In addition to the original *nudA*^{F208V} mutation as expected, we found only one additional mutation, *nudA*^{T1133S}, which is also located in the dynein tail but downstream of the previously mapped

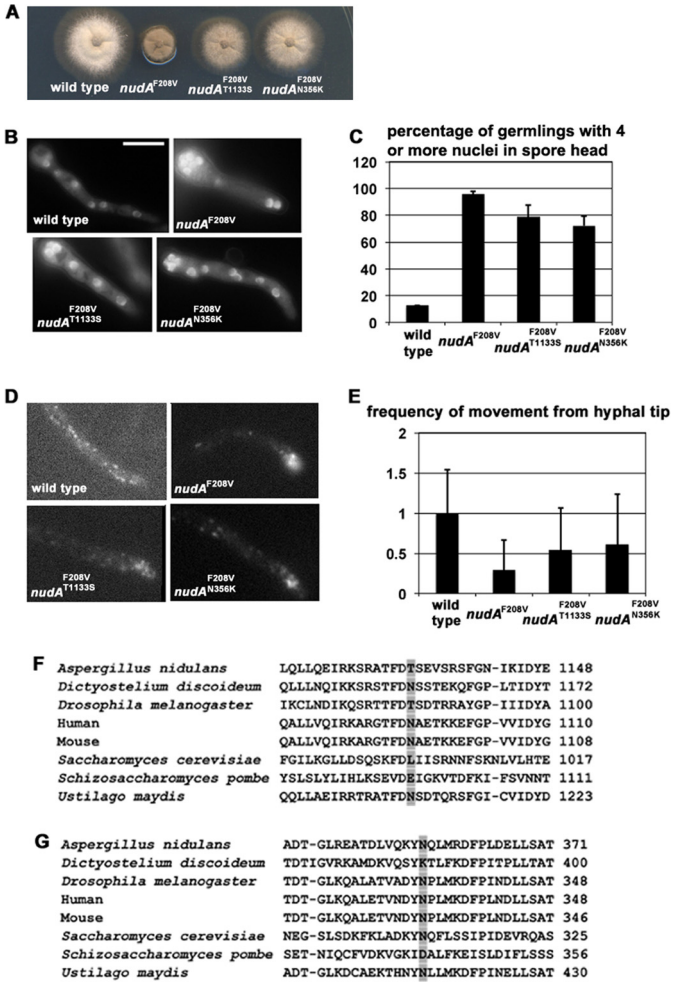

FIGURE 6. **Analyses of the two suppressors of the *nudA*^{F208V} mutant.** *A*, both the *nudA*^{N356K} and *nudA*^{T1133S} mutations partially suppress the colony phenotype of the *nudA*^{F208V} mutant. *B*, nuclear distribution phenotypes of the suppressors. *Bar*, 5 μm. *C*, a quantitative analysis of nuclear distribution in the suppressors. Percentage of cells in which the spore head contains four or more nuclei is presented. The mean and S.D. values are from data of three independent experiments ($n > 200$ DAPI-stained cells for each strain). The mean value of the *nudA*^{F208V,N356K} or *nudA*^{F208V,T1133S} mutant is lower than that of the *nudA*^{F208V} mutant ($p < 0.001$). *D*, early endosome distribution phenotypes of the suppressors. *E*, a quantitative analysis on the frequency of dynein-mediated early endosome movements. Mean and S.D. values are shown ($n = 35$ hyphal tips for wild type, $n = 45$ for the *nudA*^{F208V} mutant, $n = 49$ for the *nudA*^{F208V,N356K} mutant, and $n = 49$ for the *nudA*^{F208V,T1133S} mutant). The mean values of frequencies in the mutants within a time period of 16 s are relative to that of the wild type, which is set as 1. The mean value of the *nudA*^{F208V,N356K} or *nudA*^{F208V,T1133S} mutant is higher than that of the *nudA*^{F208V} mutant ($p < 0.001$). *F*, a sequence alignment of dynein HCs showing the position of the suppressor mutation at Thr-1133. *G*, a sequence alignment of dynein HCs showing the position of the suppressor mutation at Asn-356.

subunit interaction sites. This Thr residue is not highly conserved (Fig. 6*F*), and how this subtle mutation (Thr to Ser) influences tail structure will need to be studied in the future. Similarly, the suppressor mutation in the RQ49 strain was identified by sequencing. In addition to the original *nudA*^{F208V} mutation, one mutation, *nudA*^{N356K}, was found. This Asn residue is conserved in most species examined, but it is changed to Lys in *D. discoideum* HC and to Asp in *Schizosaccharomyces pombe* HC (Fig. 6*G*). To verify that the improved colony phenotype of the original *nudA*^{F208V} mutant was indeed caused by these mutations, we transformed the fragments containing either one of the suppressor mutations back to the original *nudA*^{F208V} mutant. Both fragments generated transformants that looked like the originally selected suppressors, and sequencing analyses of two of these suppressor-like transformants confirmed the presence of the two additional mutations. Thus, the *nudA*^{T1133S} or the *nudA*^{N356K} mutation partially compensates for the structural alteration caused by the *nudA*^{F208V} mutation.

DISCUSSION

In this study, we have identified a novel mutation, *nudA*^{F208V} in the *A. nidulans* dynein HC tail that significantly weakens dynein function in nuclear migration and early endosome movement. Although the dynein tail has been implicated in dynein subunit interactions, this mutation is located upstream of the subunit interaction sites and does not apparently affect dynein complex assembly. In the *nudA*^{F208V} mutant, early endosomes abnormally accumulate at the hyphal tip, which is indicative of a defect in dynein-mediated early endosome movement. The physical interaction between the dynein motor and the early endosome cargo is clearly not weakened. However, the frequency of dynein-mediated early endosome movement away from the hyphal tip is significantly reduced. Moreover, although some early endosomes that leave the hyphal tip move at a normal speed, some move at an abnormally low speed. Together, these results suggest that the *nudA*^{F208V} mutation causes a defect of dynein in initiating and/or sustaining cargo movement along the microtubule track *in vivo*.

Although the HC tail is not needed for motility of single dynein molecules *in vitro* as long as they are dimerized (31), the function of the tail in regulating the dynein motor has been suggested by a recent study on the *Loa* mutation in the HC tail (32). Dynein from the mouse *Loa* mutant shows a weakened dynein-microtubule interaction and a decreased motor processivity along microtubules (32). Unlike the *Loa* mutation that affects HC-IC interaction (32), the *nudA*^{F208V} mutation in *A. nidulans* does not affect HC-IC interaction and dynein complex assembly. Thus, our current result provides a strong support for the idea that besides its binding to other subunits, the tail is important for regulating dynein motor function *in vivo*. It is worth pointing out that *in vivo*, the dynein motor carrying a cargo not only needs to move in a cytoplasm with considerable viscosity (63, 64) but also needs to compete with plus-end-directed motors bound to the same cargo (65–67). In filamentous fungi, kinesin-3 is able to bind to the dynein-bound early endosome and be carried to the minus end as a cargo of dynein (40, 53, 68). In *U. maydis*, binding to a single molecule of dynein is sufficient to cause a plus-end-directed early endosome to reverse its direction (68), suggesting that dynein turns off or overpowers kinesin-3. In *A. nidulans*, however, dynein on plus-end-directed early endosomes was observed (53), suggesting that kinesin-3 is able to compete with dynein on the same cargo. In this scenario, dynein is likely to be detached from the microtubule or take backward steps as suggested by an *in vitro* study examining yeast dynein under a load that is bigger than its stall force (69). The abnormal accumulation at the hyphal tip in the *nudA*^{F208V} mutant suggests a weakened ability of the mutant dynein to compete against kinesin-3. This may have resulted from a decreased microtubule affinity during the ATPase cycle

causing the dynein motor to detach from the track or a decreased stall force causing the motor to reverse direction more frequently. Future *in vitro* work applying the optic trap technique will need to be done to address these possibilities.

Although several reports have described the structure of the HC motor domain (70–76), the structure of the tail domain has not yet been reported. Thus, how the *nudA*^{F208V} mutation affects tail structure remains unknown. However, identification of the *nudA*^{F208V} mutation and its suppressor mutations in the dynein tail indicates that the fine structure of the tail is important for motor function *in vivo*. It is interesting to note that the *nudA*^{F208I} mutation does not cause any obvious defect, suggesting that the proper size or hydrophobicity of the side chain in the Phe-208 residue is critical for function. Recently, a genetic study in another filamentous fungus *Neurospora crassa* has identified many mutations in the dynein HC that affect dynein function (77). Although most mutations are in the motor domain, two mutations, Y110S and W1308G, of the *N. crassa* HC tail have been identified (77). Interestingly, similar to the *nudA*^{F208V} mutation, the Y110S mutation is also located far upstream of the subunit interaction site. Further insights into structural roles of these involved amino acids will be generated after the structure of the tail becomes available. Exactly how a tail mutation would affect dynein motor function is unclear at this point. It has been postulated that the budding yeast dynein tail may interact with the motor domain in a way that the tail would be "masked" in the presence of the motor domain (78, 79). Interestingly, although the dynein regulator LIS1 binds to the motor domain at AAA3/AAA4 (26), removal of the tail appears to enhance dynein-LIS1 interaction (26, 31, 78). Given that the dynein HC is involved in multiple protein interactions (14–18, 21–26), it remains to be tested whether the HC tail affects dynein function directly through regulating the motor domain or indirectly through coordinating the functions of other dynein regulators.

Acknowledgments—We thank Dr. Berl Oakley and Dr. Miguel Peñalva for strains and advice on the alcA promoter-inducing conditions. We also thank Drs. Xuanli Yao and Tian Jin for helpful comments on the manuscript.

REFERENCES

1. Karki, S., and Holzbaur, E. L. (1999) Cytoplasmic dynein and dynactin in cell division and intracellular transport. *Curr. Opin. Cell Biol.* **11,** 45–53
2. Allan, V. J. (2011) Cytoplasmic dynein. *Biochem. Soc. Trans.* **39,** 1169–1178
3. Kardon, J. R., and Vale, R. D. (2009) Regulators of the cytoplasmic dynein motor. *Nat. Rev. Mol. Cell Biol.* **10,** 854–865
4. Greber, U. F., and Way, M. (2006) A superhighway to virus infection. *Cell* **124,** 741–754
5. Abe, N., and Cavalli, V. (2008) Nerve injury signaling. *Curr. Opin. Neurobiol.* **18,** 276–283
6. Vallee, R. B., Seale, G. E., and Tsai, J. W. (2009) Emerging roles for myosin II and cytoplasmic dynein in migrating neurons and growth cones. *Trends Cell Biol.* **19,** 347–355
7. Schroer, T. A. (2004) Dynactin. *Annu. Rev. Cell Dev. Biol.* **20,** 759–779
8. Wynshaw-Boris, A. (2007) Lissencephaly and LIS1: insights into the molecular mechanisms of neuronal migration and development. *Clin. Genet.* **72,** 296–304
9. Perlson, E., Maday, S., Fu, M. M., Moughamian, A. J., and Holzbaur, E. L. (2010) Retrograde axonal transport: pathways to cell death? *Trends Neurosci.* **33,** 335–344
10. Asai, D. J., and Koonce, M. P. (2001) The dynein heavy chain: structure, mechanics and evolution. *Trends Cell Biol.* **11,** 196–202
11. King, S. M. (2000) AAA domains and organization of the dynein motor unit. *J. Cell Sci.* **113,** 2521–2526
12. Roberts, A. J., Numata, N., Walker, M. L., Kato, Y. S., Malkova, B., Kon, T., Ohkura, R., Arisaka, F., Knight, P. J., Sutoh, K., and Burgess, S. A. (2009) AAA+ Ring and linker swing mechanism in the dynein motor. *Cell* **136,** 485–495
13. Höök, P., and Vallee, R. (2012) Dynein dynamics. *Nat. Struct. Mol. Biol.* **19,** 467–469
14. Pfister, K. K., Shah, P. R., Hummerich, H., Russ, A., Cotton, J., Annuar, A. A., King, S. M., and Fisher, E. M. (2006) Genetic analysis of the cytoplasmic dynein subunit families. *PLoS Genet.* **2,** e1
15. Karki, S., and Holzbaur, E. L. (1995) Affinity chromatography demonstrates a direct binding between cytoplasmic dynein and the dynactin complex. *J. Biol. Chem.* **270,** 28806–28811
16. Vaughan, K. T., and Vallee, R. B. (1995) Cytoplasmic dynein binds dynactin through a direct interaction between the intermediate chains and p150Glued. *J. Cell Biol.* **131,** 1507–1516
17. King, S. J., Brown, C. L., Maier, K. C., Quintyne, N. J., and Schroer, T. A. (2003) Analysis of the dynein-dynactin interaction *in vitro* and *in vivo*. *Mol. Biol. Cell* **14,** 5089–5097
18. Susalka, S. J., Nikulina, K., Salata, M. W., Vaughan, P. S., King, S. M., Vaughan, K. T., and Pfister, K. K. (2002) The roadblock light chain binds a novel region of the cytoplasmic Dynein intermediate chain. *J. Biol. Chem.* **277,** 32939–32946
19. Efimov, V. P., and Morris, N. R. (2000) The LIS1-related NUDF protein of *Aspergillus nidulans* interacts with the coiled-coil domain of the NUDE/RO11 protein. *J. Cell Biol.* **150,** 681–688
20. Shu, T., Ayala, R., Nguyen, M. D., Xie, Z., Gleeson, J. G., and Tsai, L. H. (2004) Ndel1 operates in a common pathway with LIS1 and cytoplasmic dynein to regulate cortical neuronal positioning. *Neuron* **44,** 263–277
21. McKenney, R. J., Vershinin, M., Kunwar, A., Vallee, R. B., and Gross, S. P. (2010) LIS1 and NudE induce a persistent dynein force-producing state. *Cell* **141,** 304–314
22. Wang, S., and Zheng, Y. (2011) Identification of a novel dynein binding domain in nudel essential for spindle pole organization in *Xenopus* egg extract. *J. Biol. Chem.* **286,** 587–593
23. McKenney, R. J., Weil, S. J., Scherer, J., and Vallee, R. B. (2011) Mutually exclusive cytoplasmic dynein regulation by NudE-Lis1 and dynactin. *J. Biol. Chem.* **286,** 39615–39622
24. Zylkiewicz, E., Kijańska, M., Choi, W. C., Derewenda, U., Derewenda, Z. S., and Stukenberg, P. T. (2011) The N-terminal coiled-coil of Ndel1 is a regulated scaffold that recruits LIS1 to dynein. *J. Cell Biol.* **192,** 433–445
25. Nyarko, A., Song, Y., and Barbar, E. (2012) Intrinsic disorder in dynein intermediate chain modulates its interactions with NudE and dynactin. *J. Biol. Chem.* **287,** 24884–24893
26. Huang, J., Roberts, A. J., Leschziner, A. E., and Reck-Peterson, S. L. (2012) Lis1 acts as a "clutch" between the ATPase and microtubule-binding domains of the dynein motor. *Cell* **150,** 975–986
27. Burgess, S. A., Walker, M. L., Sakakibara, H., Knight, P. J., and Oiwa, K. (2003) Dynein structure and power stroke. *Nature* **421,** 715–718
28. Shima, T., Kon, T., Imamula, K., Ohkura, R., and Sutoh, K. (2006) Two modes of microtubule sliding driven by cytoplasmic dynein. *Proc. Natl. Acad. Sci. U.S.A.* **103,** 17736–17740
29. Numata, N., Kon, T., Shima, T., Imamula, K., Mogami, T., Ohkura, R., Sutoh, K., and Sutoh, K. (2008) Molecular mechanism of force generation by dynein, a molecular motor belonging to the AAA+ family. *Biochem. Soc. Trans.* **36,** 131–135
30. Roberts, A. J., Malkova, B., Walker, M. L., Sakakibara, H., Numata, N., Kon, T., Ohkura, R., Edwards, T. A., Knight, P. J., Sutoh, K., Oiwa, K., and Burgess, S. A. (2012) ATP-driven remodeling of the linker domain in the dynein motor. *Structure* **20,** 1670–1680
31. Reck-Peterson, S. L., Yildiz, A., Carter, A. P., Gennerich, A., Zhang, N., and Vale, R. D. (2006) Single-molecule analysis of dynein processivity and stepping behavior. *Cell* **126,** 335–348

32. Ori-McKenney, K. M., Xu, J., Gross, S. P., and Vallee, R. B. (2010) A cytoplasmic dynein tail mutation impairs motor processivity. *Nat. Cell Biol.* **12,** 1228–1234
33. Sivagurunathan, S., Schnittker, R. R., Nandini, S., Plamann, M. D., and King, S. J. (2012) A mouse neurodegenerative dynein heavy chain mutation alters dynein motility and localization in *Neurospora crassa*. *Cytoskeleton* **69,** 613–624
34. Deng, W., Garrett, C., Dombert, B., Soura, V., Banks, G., Fisher, E. M., van der Brug, M. P., and Hafezparast, M. (2010) Neurodegenerative mutation in cytoplasmic dynein alters its organization and dynein-dynactin and dynein-kinesin interactions. *J. Biol. Chem.* **285,** 39922–39934
35. Peñalva, M. A., Galindo, A., Abenza, J. F., Pinar, M., Calcagno-Pizarelli, A. M., Arst, H. N., and Pantazopoulou, A. (2012) Searching for gold beyond mitosis: Mining intracellular membrane traffic in *Aspergillus nidulans*. *Cell. Logist.* **2,** 2–14
36. Xiang, X. (2011) Insights into cytoplasmic dynein function and regulation from fungal genetics in *Dyneins: Structure, Biology and Disease* (King, S. M., ed.) pp. 455–481, Elsevier. Maryland Heights, MO
37. Steinberg, G. (2011) Motors in fungal morphogenesis: cooperation versus competition. *Curr. Opin. Microbiol.* **14,** 660–667
38. Egan, M. J., McClintock, M. A., and Reck-Peterson, S. L. (2012) *Curr. Opin. Microbiol.*, **15,** 637–645
39. Xiang, X., Osmani, A. H., Osmani, S. A., Xin, M., and Morris, N. R. (1995) NudF, a nuclear migration gene in *Aspergillus nidulans*, is similar to the human LIS-1 gene required for neuronal migration. *Mol. Biol. Cell* **6,** 297–310
40. Lenz, J. H., Schuchardt, I., Straube, A., and Steinberg, G. (2006) A dynein loading zone for retrograde endosome motility at microtubule plus-ends. *EMBO J.* **25,** 2275–2286
41. Han, G., Liu, B., Zhang, J., Zuo, W., Morris, N. R., and Xiang, X. (2001) The *Aspergillus* cytoplasmic dynein heavy chain and NUDF localize to microtubule ends and affect microtubule dynamics. *Curr. Biol.* **11,** 719–724
42. Lee, W. L., Oberle, J. R., and Cooper, J. A. (2003) The role of the lissencephaly protein Pac1 during nuclear migration in budding yeast. *J. Cell Biol.* **160,** 355–364
43. Sheeman, B., Carvalho, P., Sagot, I., Geiser, J., Kho, D., Hoyt, M. A., and Pellman, D. (2003) Determinants of *S. cerevisiae* dynein localization and activation: implications for the mechanism of spindle positioning. *Curr. Biol.* **13,** 364–372
44. Splinter, D., Razafsky, D. S., Schlager, M. A., Serra-Marques, A., Grigoriev, I., Demmers, J., Keijzer, N., Jiang, K., Poser, I., Hyman, A. A., Hoogenraad, C. C., King, S. J., and Akhmanova, A. (2012) BICD2, dynactin, and LIS1 cooperate in regulating dynein recruitment to cellular structures. *Mol. Biol. Cell* **23,** 4226–4241
45. Abenza, J. F., Pantazopoulou, A., Rodríguez, J. M., Galindo, A., and Peñalva, M. A. (2009) Long-distance movement of *Aspergillus nidulans* early endosomes on microtubule tracks. *Traffic* **10,** 57–75
46. Zekert, N., and Fischer, R. (2009) The *Aspergillus nidulans* kinesin-3 UncA motor moves vesicles along a subpopulation of microtubules. *Mol. Biol. Cell* **20,** 673–684
47. Zhang, J., Zhuang, L., Lee, Y., Abenza, J. F., Peñalva, M. A., and Xiang, X. (2010) The microtubule plus-end localization of *Aspergillus* dynein is important for dynein-early-endosome interaction but not for dynein ATPase activation. *J. Cell Sci.* **123,** 3596–3604
48. Zhang, J., Han, G., and Xiang, X. (2002) Cytoplasmic dynein intermediate chain and heavy chain are dependent upon each other for microtubule end localization in *Aspergillus nidulans*. *Mol. Microbiol.* **44,** 381–392
49. Zhang, J., Li, S., Fischer, R., and Xiang, X. (2003) Accumulation of cytoplasmic dynein and dynactin at microtubule plus ends in *Aspergillus nidulans* is kinesin dependent. *Mol. Biol. Cell* **14,** 1479–1488
50. Zhang, J., Li, S., Musa, S., Zhou, H., and Xiang, X. (2009) Dynein light intermediate chain in *Aspergillus nidulans* is essential for the interaction between heavy and intermediate chains. *J. Biol. Chem.* **284,** 34760–34768
51. Zhang, J., Wang, L., Zhuang, L., Huo, L., Musa, S., Li, S., and Xiang, X. (2008) Arp11 affects dynein-dynactin interaction and is essential for dynein function in *Aspergillus nidulans*. *Traffic* **9,** 1073–1087
52. Yao, X., Zhang, J., Zhou, H., Wang, E., and Xiang, X. (2012) *In vivo* roles of the basic domain of dynactin p150 in microtubule plus-end tracking and dynein function. *Traffic* **13,** 375–387
53. Egan, M. J., Tan, K., and Reck-Peterson, S. L. (2012) Lis1 is an initiation factor for dynein-driven organelle transport. *J. Cell Biol.* **197,** 971–982
54. Willins, D. A., Xiang, X., and Morris, N. R. (1995) An α tubulin mutation suppresses nuclear migration mutations in *Aspergillus nidulans*. *Genetics* **141,** 1287–1298
55. Xiang, X., Zuo, W., Efimov, V. P., and Morris, N. R. (1999) Isolation of a new set of *Aspergillus nidulans* mutants defective in nuclear migration. *Current genetics* **35,** 626–630
56. Nayak, T., Edgerton-Morgan, H., Horio, T., Xiong, Y., De Souza, C. P., Osmani, S. A., and Oakley, B. R. (2010) γ-Tubulin regulates the anaphase-promoting complex/cyclosome during interphase. *J. Cell Biol.* **190,** 317–330
57. Zhuang, L., Zhang, J., and Xiang, X. (2007) Point mutations in the stem region and the fourth AAA domain of cytoplasmic dynein heavy chain partially suppress the phenotype of NUDF/LIS1 loss in *Aspergillus nidulans*. *Genetics* **175,** 1185–1196
58. Xiang, X., Roghi, C., and Morris, N. R. (1995) Characterization and localization of the cytoplasmic dynein heavy chain in *Aspergillus nidulans*. *Proc. Natl. Acad. Sci. U.S.A.* **92,** 9890–9894
59. Zhang, J., Yao, X., Fischer, L., Abenza, J. F., Peñalva, M. A., and Xiang, X. (2011) The p25 subunit of the dynactin complex is required for dynein-early endosome interaction. *J. Cell Biol.* **193,** 1245–1255
60. Tynan, S. H., Gee, M. A., and Vallee, R. B. (2000) Distinct but overlapping sites within the cytoplasmic dynein heavy chain for dimerization and for intermediate chain and light intermediate chain binding. *J. Biol. Chem.* **275,** 32769–32774
61. Habura, A., Tikhonenko, I., Chisholm, R. L., and Koonce, M. P. (1999) Interaction mapping of a dynein heavy chain. Identification of dimerization and intermediate-chain binding domains. *J. Biol. Chem.* **274,** 15447–15453
62. Yeh, T. Y., Quintyne, N. J., Scipioni, B. R., Eckley, D. M., and Schroer, T. A. (2012) Dynactin's pointed-end complex is a cargo-targeting module. *Mol. Biol. Cell* **23,** 3827–3837
63. Bloom, K. S. (2008) Beyond the code: the mechanical properties of DNA as they relate to mitosis. *Chromosoma* **117,** 103–110
64. Hendricks, A. G., Holzbaur, E. L., and Goldman, Y. E. (2012) Force measurements on cargoes in living cells reveal collective dynamics of microtubule motors. *Proc. Natl. Acad. Sci. U.S.A.* **109,** 18447–18452
65. Soppina, V., Rai, A. K., Ramaiya, A. J., Barak, P., and Mallik, R. (2009) Tug-of-war between dissimilar teams of microtubule motors regulates transport and fission of endosomes. *Proc. Natl. Acad. Sci. U.S.A.* **106,** 19381–19386
66. Hendricks, A. G., Perlson, E., Ross, J. L., Schroeder, H. W., 3rd, Tokito, M., and Holzbaur, E. L. (2010) Motor coordination via a tug-of-war mechanism drives bidirectional vesicle transport. *Curr. Biol.* **20,** 697–702
67. Leidel, C., Longoria, R. A., Gutierrez, F. M., and Shubeita, G. T. (2012) Measuring molecular motor forces *in vivo*: implications for tug-of-war models of bidirectional transport. *Biophys. J.* **103,** 492–500
68. Schuster, M., Lipowsky, R., Assmann, M. A., Lenz, P., and Steinberg, G. (2011) Transient binding of dynein controls bidirectional long-range motility of early endosomes. *Proc. Natl. Acad. Sci. U.S.A.* **108,** 3618–3623
69. Gennerich, A., Carter, A. P., Reck-Peterson, S. L., and Vale, R. D. (2007) Force-induced bidirectional stepping of cytoplasmic dynein. *Cell* **131,** 952–965
70. McNaughton, L., Tikhonenko, I., Banavali, N. K., LeMaster, D. M., and Koonce, M. P. (2010) A low affinity ground state conformation for the Dynein microtubule binding domain. *J. Biol. Chem.* **285,** 15994–16002
71. Carter, A. P., Cho, C., Jin, L., and Vale, R. D. (2011) Crystal structure of the dynein motor domain. *Science* **331,** 1159–1165
72. Kon, T., Sutoh, K., and Kurisu, G. (2011) X-ray structure of a functional full-length dynein motor domain. *Nat. Struct. Mol. Biol.* **18,** 638–642
73. Kon, T., Oyama, T., Shimo-Kon, R., Imamula, K., Shima, T., Sutoh, K., and Kurisu, G. (2012) The 2.8 Å crystal structure of the dynein motor domain. *Nature* **484,** 345–350
74. Schmidt, H., Gleave, E. S., and Carter, A. P. (2012) Insights into dynein motor domain function from a 3.3-Å crystal structure. *Nat. Struct. Mol. Biol.* **19,** 492–497

75. Billington, N., and Sellers, J. R. (2011) Dynein struts its stuff. *Nat. Struct. Mol. Biol.* **18,** 635–636
76. Redwine, W. B., Hernández-López, R., Zou, S., Huang, J., Reck-Peterson, S. L., and Leschziner, A. E. (2012) Structural basis for microtubule binding and release by dynein. *Science* **337,** 1532–1536
77. Sivagurunathan, S., Schnittker, R. R., Razafsky, D. S., Nandini, S., Plamann, M. D., and King, S. J. (2012) Analyses of dynein heavy chain mutations reveal complex interactions between dynein motor domains and cellular dynein functions. *Genetics* **191,** 1157–1179
78. Markus, S. M., Punch, J. J., and Lee, W. L. (2009) Motor- and tail-dependent targeting of dynein to microtubule plus ends and the cell cortex. *Curr. Biol.* **19,** 196–205
79. Markus, S. M., and Lee, W. L. (2011) Regulated offloading of cytoplasmic dynein from microtubule plus ends to the cortex. *Dev. Cell* **20,** 639–651
80. Nayak, T., Szewczyk, E., Oakley, C. E., Osmani, A., Ukil, L., Murray, S. L., Hynes, M. J., Osmani, S. A., and Oakley, B. R. (2006) A versatile and efficient gene-targeting system for *Aspergillus nidulans*. *Genetics* **172,** 1557–1566